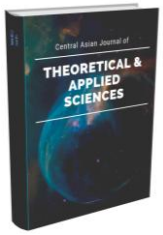

CENTRAL ASIAN JOURNAL OF THEORETICAL AND APPLIED SCIENCE

https://cajotas.centralasianstudies.org/index.php/CAJOTAS

Volume: 07 Issue: 03 | July 2026 ISSN: 2660-5317

Article

Synthesis, Characterization, and Molecular Docking of Cefoxitin-Derived Schiff Bases: Biological Activity and Thermal Stability (TGA)

Anaam Khalif Al-Azzawy[1], Diaa M. Najim[2], Mohammad M. Al-Tufah[3]

1. Salah Al-Din Education Directorate, Iraq
2. Kirkuk Education Directorate, Iraq
3. Directorate of Education, Kirkuk, Ministry of Education, Iraq

*** Correspondence:** anaam.k.athab@st.tu.edu.iq[1], info@researchcenter.iq[2], Mohamadmd282@gmail.com[3]

Abstract: In this study, new Schiff base derivatives were prepared via addition and condensation reactions by adding cefoxitin to substituted benzaldehydes or ketones in an acidic medium. To produce Schiff bases (D1-D4), cefoxitin was added to the carbonyl compounds in the presence of ethanol as a solvent, using glacial acetic acid as a catalyst. The structures of the prepared compounds were determined using FT-IR spectroscopy and, for some of them, 1H-NMR and 13C-NMR spectroscopy. The biological activity of prepared Schiff bases (D1-D4) was studied against G-negative bacteria (Klebsiella and Pseudomonas aeruginosa) and G-positive bacteria (Enterococcus faecalis and Staphylococcus aureus). The results showed antibacterial activity of the prepared compounds at high concentrations (0.01 and 0.001 mg/ml) compared to low concentrations (0.001 mg/ml) against Staphylococcus aureus, Enterococcus faecalis, and Klebsiella due to the effect of high concentration. In addition to performing the GTA thermal decomposition of compounds D1 and D3 to measure the change in the mass of these compounds with increasing temperatures and determine their thermal stability. In addition, compounds D1 and D3 underwent GTA thermal decomposition to assess the mass change of these compounds as temperatures increased and establish their thermal stability. Molecular docking of the three compounds (D2 and D3) with the target protein (8C7Y) was carried out using the MOE software. With the target protein, all compounds exhibited high binding affinity values. With important amino acid residues in the active site, hydrogen bonding and hydrophobic interactions were the primary interaction types.

Keywords: Cefoxitin, Schiff bases, biological activities, thermal Analysis, Molecular docking.

Citation: Al-Azzawy A. K., Najim D. M., Al-Tufah M. M. Synthesis, Characterization, and Molecular Docking of Cefoxitin-Derived Schiff Bases: Biological Activity and Thermal Stability (TGA). Central Asian Journal of Theoretical and Applied Science 2026, 7(3), 67-85.

Received: 10th Feb 2026
Revised: 11th Mar 2026
Accepted: 24th Apr 2026
Published: 22th May 2026

Introduction

The first to isolate cephalosporins was the Italian scientist Giuseppe Bruzzo in 1948 from cultures of the fungus Cephalosporium acrimonium. These compounds are structurally and functionally related to penicillins and are derived from aminocephalosporic acid. Cephalosporins consist of a hexagonal ring containing a sulfur atom connected to a beta-lactam ring. Cefoxitin is classified as a second-generation antibiotic[1]. Cefixime has a molecular weight 453.4 and has molecular formula $C_{16}H_{15}N_5O_7S_2$[2]. Cefoxitin acid (6R,7S)-3-((carbamoyloxy)methyl)-7-methoxy-8-oxo-7-(2-(thiophen-2-yl)acetamido)-5-thia-1-

azabicyclo[4.2.0]oct-2-ene-2-carboxylic acid (Figure 1) is a semi-synthetic cephamycin and possesses important biochemical characteristics that are not found in other β-lactam antibiotics due to its 7c-methoxyl group[3, 4]. Cefoxitin compounds contain a methoxy group that reduces the hydrolysis process in bacteria by beta-lactamase, so they are less dangerous than other second-generation cephalosporins in terms of drug resistance, although the action of cefoxitin is similar to that of cephalosporins[5, 6]. Cefoxitin is commonly recommended and used for perioperative parenteral surgical prophylaxis in colorectal, abdominal, pelvic, bariatric, and gynecologic surgical procedures[7, 8]. Schiff bases are organic compounds produced by the condensation reaction between primary amines and carbonyl compounds (aldehydes and ketones). Because they contain carbon-nitrogen double bonds (-C=N-), they are of importance in medicine and pharmacology[9, 10]. Structurally, Schiff bases are known as imines or azomethines and are expressed structurally by the formula RHC=N–R_1, R_1 and R may be an alkyl group, aryl group, or heterocycles[11, 12]. The imine group, which contains electrophilic carbon and nucleophilic nitrogen, provides excellent binding opportunities with different nucleophiles and electrophiles, thereby inhibiting targeted diseases, enzymes, or DNA replication[10]. Schiff bases, especially those linked with a heterocyclic moiety, exhibited various pharmacological and biological activities[13]. such as antibacterial[14], antioxidant[4], antifungal[15], antimalarial[16], anticonvulsant[17], and anti-inflammatory[18]. This study aims to synthesize and characterize new Schiff base derivatives derived from the antibiotic cefoxitin and subsequently investigate their thermal properties with the help of thermogravimetric analysis (TGA) in order to identify stages of degradation and physicochemical stability. Also, in this study, the structures showing the highest affinity for target proteins have been identified using molecular docking simulations to calculate the binding energy between the native ligand and its derivatives, thereby elucidating the structural-activity relationship of these derivatives.

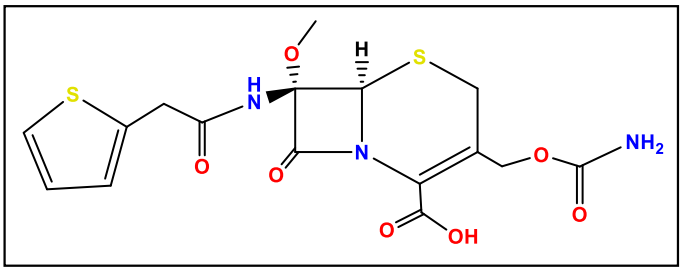

Figure 1: structure of Cephalosporin.

Materials and Methods

4 -Bromobenzaldehyde, 4-Fluorobenzaldehyde, 4-Nitroacetophenone, 4-Chloroacetophenone, ethanol, hydroxylamine hydrochloride, acetic acid, anhydrous sodium sulfate, and sodium acetate are sourced from Fluka and Aldrich and utilized without additional purification. Melting points of the compounds were measured by a melting point apparatus (uncorrected). Using a Perkin-Elmer 1650 spectrometer (400-4000)cm-1 in KBr disks, FT-IR spectra were captured. Tetramethylsilane (TMS) was used as an internal standard for recording ^{1}H-NMR and ^{13}C-NMR spectra of a solution in dimethyl sulphoxide (DMSO-d_6) at ambient temperature, utilizing Bruker spectroscopic ultra-shield magnets on a 300 MHz spectrometer. Simultaneous Differential Thermal Analysis (SDT) Q600 Build 20 was used to measure the thermal stability of some compounds.

Synthesis of Schiff bases (D_1-D_4)[19]

Cefoxitin 4.7 g (0.01 mol) was dissolved in 6 drops of glacial acetic acid and 20 ml of ethanol. In a 100 ml round-bottom flask under continuous stirring at room temperature. The experiment was conducted as four parallel reactions. In the first reaction, 4-bromobenzaldehyde 1.85 g (0.01 mol) was added to the solution, while in the other three reactions, 4-bromobenzaldehyde, 1.85 g (0.01 mol), 4-nitroacetophenone, 1.65 g (0.01 mol), and chloroacetophenone 1.54 g (0.01 mol) were added, respectively, under the same condition. Then, 1 g (0.007 mol) of anhydrous sodium sulfate (Na_2SO_4) was added to each mixture as a drying agent. The mixtures were refluxed for 4 hours at 80 °C. The resulting precipitate was collected by filtration and recrystallized from ethanol. Table 1 shows the physical properties of the derivative (D_1-D_4).

Table 1: The synthesized compounds physical characteristics (D_1-D_4)

Compound No.	X	R_1	R_2	Molecular Formula	Color	M.P. ^OC	Yield %
D_1	C	H	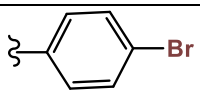	$C_{23}H_{20}BrN_3O_7S_2$	White	175-177Dec.	78%
D_2	C	H	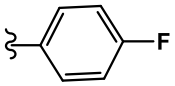	$C_{23}H_{20}FN_3O_7S_2$	Light Blue	164-166 Dec.	76%
D_3	C	CH_3	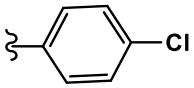	$C_{24}H_{22}ClN_3O_7S_2$	Light Brown	167-169 Dec.	74%
D_4	C	CH_3	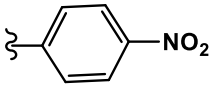	$C_{24}H_{22}N_4O_9S_2$	Red	137-139	71%

Results and Discussion:

Cefoxitin Schiff bases were prepared using cefoxitin as the starting material. Cefoxitin was mixed with an equimolar amount of the respective aldehyde or ketone in ethanol. The resulting mixtures were refluxed for 8 hours to yield the desired product. Scheme 1.

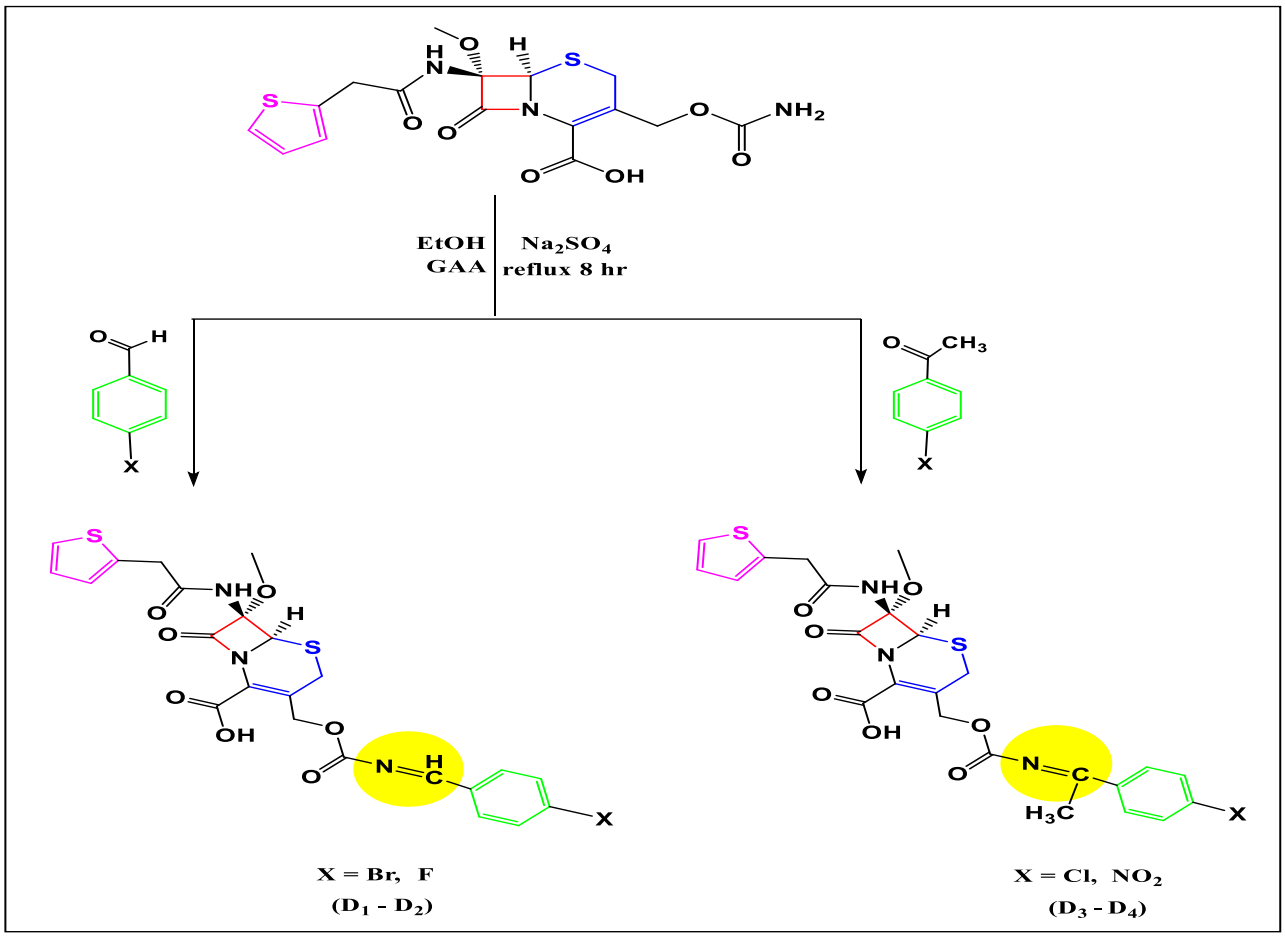

Scheme 1: Compound synthesis pathway (D_1-D_4).

FT-IR spectrum interpretation.

The FT-IR spectrum of the compound D_1 (see Table 1 and Figure 2) confirmed the successful synthesis. The disappearance of the amine (NH_2) band indicates its involvement in the reaction. The spectrum displays key absorption bands at: 3308 cm^{-1} for the amide group (N-H) stretch[20], 2500-3500 cm^{-1} for the hydroxyl group (OH) stretch[21], 2965 and 2884 cm-1 for the aliphatic υ(C-H) stretch[22], 1765 cm^{-1} for the lactam group (C=O), 1719 cm^{-1} for the carboxylic acid group (C=O), 1682 cm^{-1} for the amide group υ(C=O), and 1622 cm^{-1} for the imine group υ(C=N).

The FT-IR spectrum of the compound D_3 (see Table 1 and Figure 3) displays the key absorption bands at 3435 cm^{-1} for the amide group (N-H) stretch[23], 2500-3200 cm^{-1} for the hydroxyl group (OH) stretch, 3073 cm^{-1} for the aromatic υ(C-H) stretch, 2916 and 2841 cm^{-1} for the aliphatic υ(C-H) stretch, 1776 cm^{-1} lactam group (C=O) [16, 24] (Anacona & Gil, 2005; Kumar et al., 2011) (Anacona & Gil, 2005; Kumar et al., 2011) (Anacona & Gil, 2005; Kumar et al., 2011) (Anacona & Gil, 2005; Kumar et al., 2011) (Anacona & Gil, 2005; Kumar et al., 2011) (Anacona & Gil, 2005; Kumar et al., 2011) (Anacona & Gil, 2005; Kumar et al., 2011) (Anacona & Gil, 2005; Kumar et al., 2011), 1730 cm^{-1} attributed to the carboxylic acid group (C=O), 1670 cm^{-1} due to the amide group υ(C=O)[25], and 1570 cm^{-1} for the imine group υ(C=N).

Table 2: FT-IR values for the compounds (D_1-D_4)

Compound No.	IR(KBr) υ . (cm^{-1})							
	υ (N-H)	υ (OH)	υ (C-H) aromatic	υ (C=O) lactam	υ (C=O) carboxyilic acid	υ (C=O) amide	υ (C=N) imine	Other absorptions
D_1	3308	2500-3500	3086	1765	1719	1682	1622	υ (C-Br) 635 cm-1
D_2	3376	2500-3300	3044	1744	1722	1655	1661	υ (C-Cl) 744 cm-1
D_3	3435	2500-3200	3073	1776	1730	1670	1570	υ (C-NO_2) 1326,1456 cm-1
D_4	3277	2500-3500	3067	1736	1723	1687	1644	υ (C-H)aliphtic 2970, 2833cm^{-1}

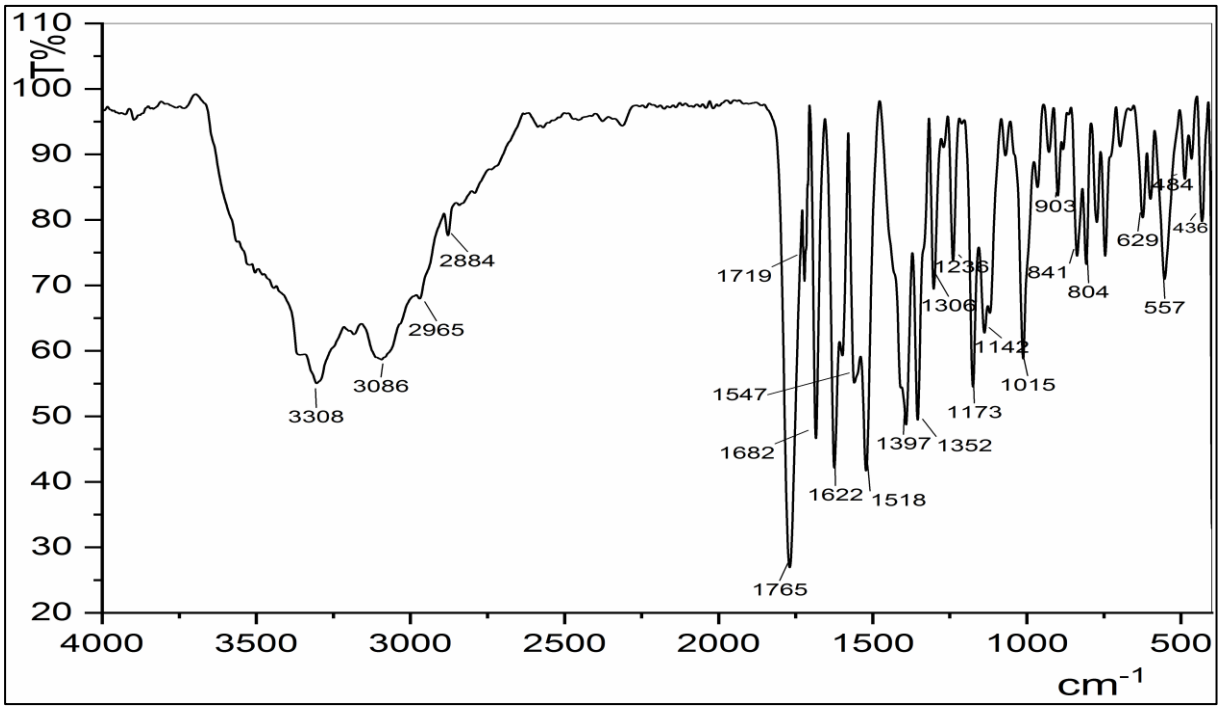

Figure 2: The infrared spectrum of D_1.

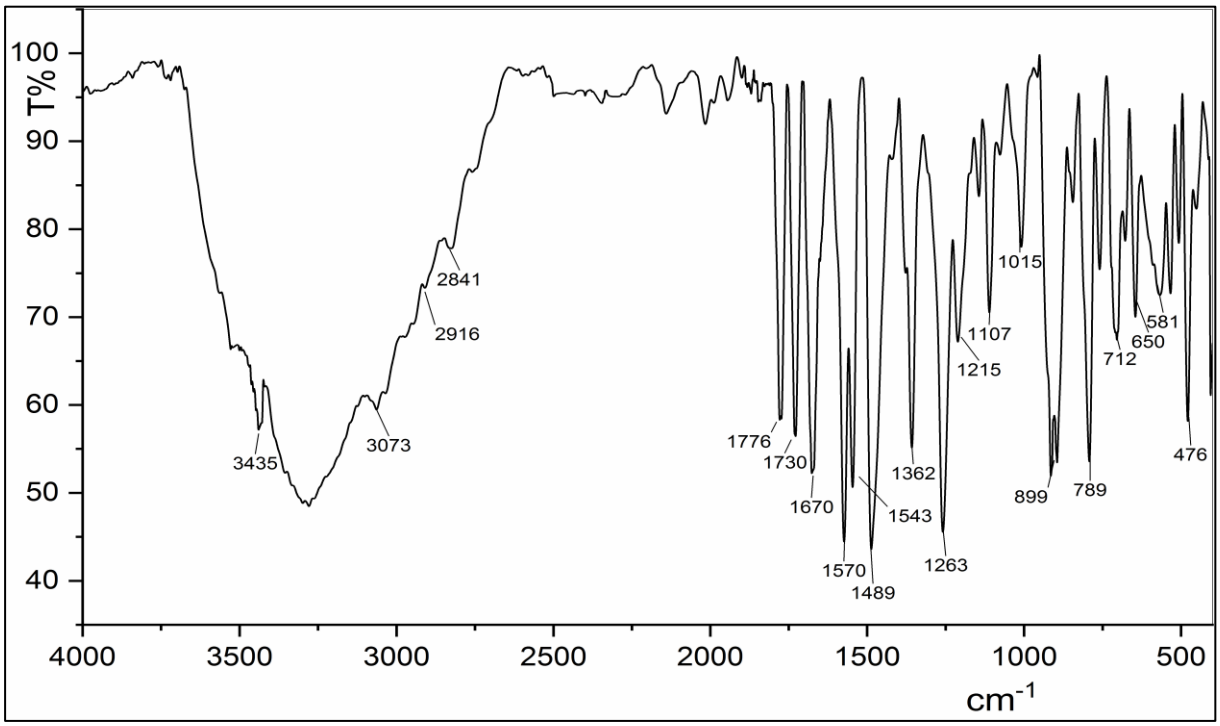

Figure 3: The infrared spectrum of D_3.

1H-NMR spectrum interpretation.

Showed ^{1}H-NMR of spectrum compound D_1 (Figure 4), which revealed a single signal at 2.94 ppm, due to the methylene proton (2H, S-CH_2); a doublet signal appeared at 3.68 ppm attributed to the methoxy proton (3H, OCH_3); another doublet signal at 3.76 ppm returned to the methylene proton (2H, CH_2-CO-); a doublet signal at 6.79 ppm due to the methylene proton (3H, CH_2-O); and a doublet signal at 6.81 ppm related to the methine proton (H, S-CH-N). A series of signals in the ring (6.84-6.99 ppm) are assigned to the protons of the thiophene ring[26], characteristic of the aromatic proton (Ar-H) at (7.33-8.10 ppm), a single signal at 9.79 ppm attributed to the imine proton (H, CH=N), a single signal at 10.09 ppm attributed to the amine proton (H, NH), and a single signal at 12.14 ppm attributed to the hydroxy proton (H, OH).

Showed ^{1}H-NMR of compound D_3 (Figure 5), which revealed a single signal at 2.40 ppm assigned to the methyl proton (3H, CH_3), and another single signal at 2.87 ppm, assigned to the methylene proton (2H, S-CH_2), a doublet signal at 4.16 ppm attributed to the methoxy proton (3H, OCH_3), and another doublet signal at 4.24 ppm due to the methylene proton (2H, CH_2-CO-); a doublet signal appeared at 6.74 ppm returning to the methylene protons (3H, CH_2-O). A series of signals in the ring (6.91-6.93 ppm) are assigned to the protons of the thiophene ring, characteristic of the aromatic proton (Ar-H) at (7.19-8.71 ppm), a single signal at 9.76 ppm due to the amine proton (H, NH), and a single signal at 12.13 ppm attributed to the hydroxy proton (H, OH)[6].

^{13}C-NMR spectrum interpretation.

The ^{13}C-NMR spectrum of compound D_1 (Figure 6) showed a signal at 29.2 ppm, assigned to the carbon of the methylene group (S-CH_2); a signal at 31.35 ppm, assigned to the carbon of the methoxy group (OCH_3); a signal at 64.3 ppm, attributed to the carbon of the methylene group (O-CH_2); a signal at 144 ppm, assigned to the carbonyl carbon (O-CO-N); a signal at 145 ppm, assigned to the carboxyl carbon (CO-OH); a signal at 158 ppm related to the azomethine carbon group (C=N); a signal at 173 ppm, due to the lactam carbon (CO), and a signal at

174 ppm, 174 ppm. A series of signals in the ring (115-143 ppm) are assigned to the carbons of the thiophene ring and aromatic ring.

The ^{13}C-NMR spectrum of compound D_3 (Figure 7) showed a signal at 29.2 ppm, due to the carbon of the methyl group (CH_3); a signal at 29.3 ppm, related to the carbon of the methylene group (S-CH_2); a signal at 31.2 ppm, returning to the carbon of the methoxy group (OCH_3); a signal at 55.5 ppm, assigned to the carbon of the methylene group (O-CH_2); a signal at 155 ppm, due to the carbonyl carbon (O-CO-N); a signal at 157 ppm, assigned to the carboxyl carbon (CO-OH); a signal at 169 ppm, returning to the lactam carbon (CO); a signal at 173 ppm, attributed to the amide carbon group (-CO-NH); and a signal at 174 ppm, due to the azomethine carbon group (C=N). A series of signals in the ring (114-145) ppm are assigned to the carbons of the thiophene ring and aromatic ring.

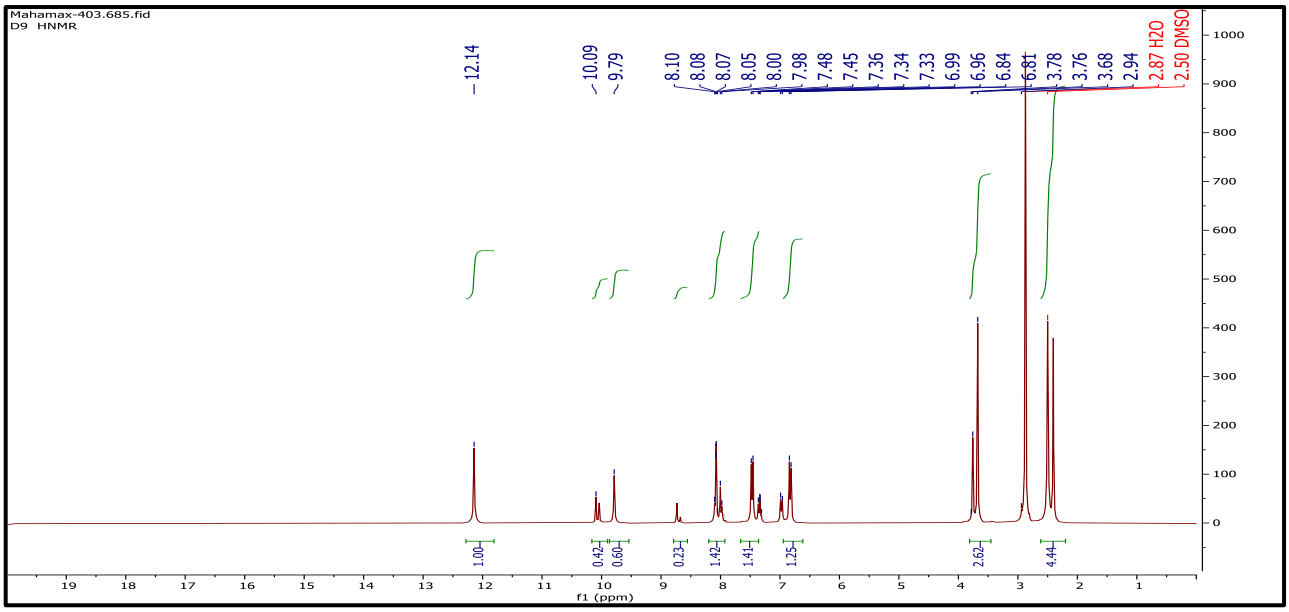

Figure 4: 1H-NMR spectra of the compound (D_1)

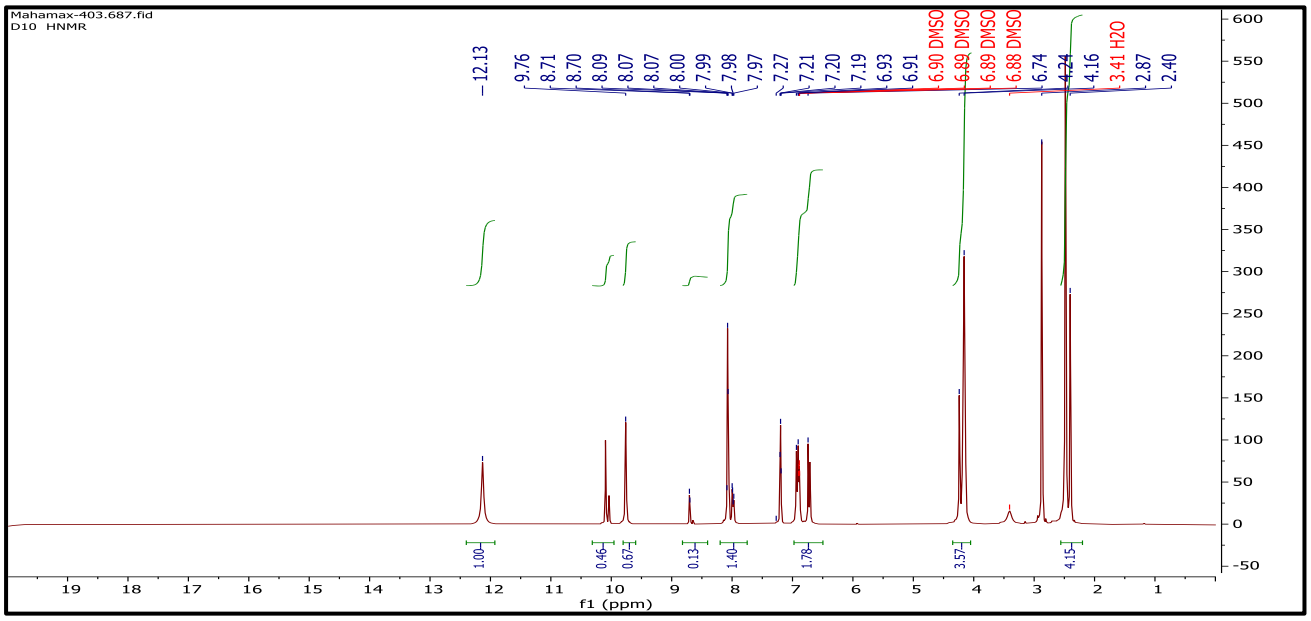

Figure 5: ^{1}H-NMR spectra of the compound (D_3)

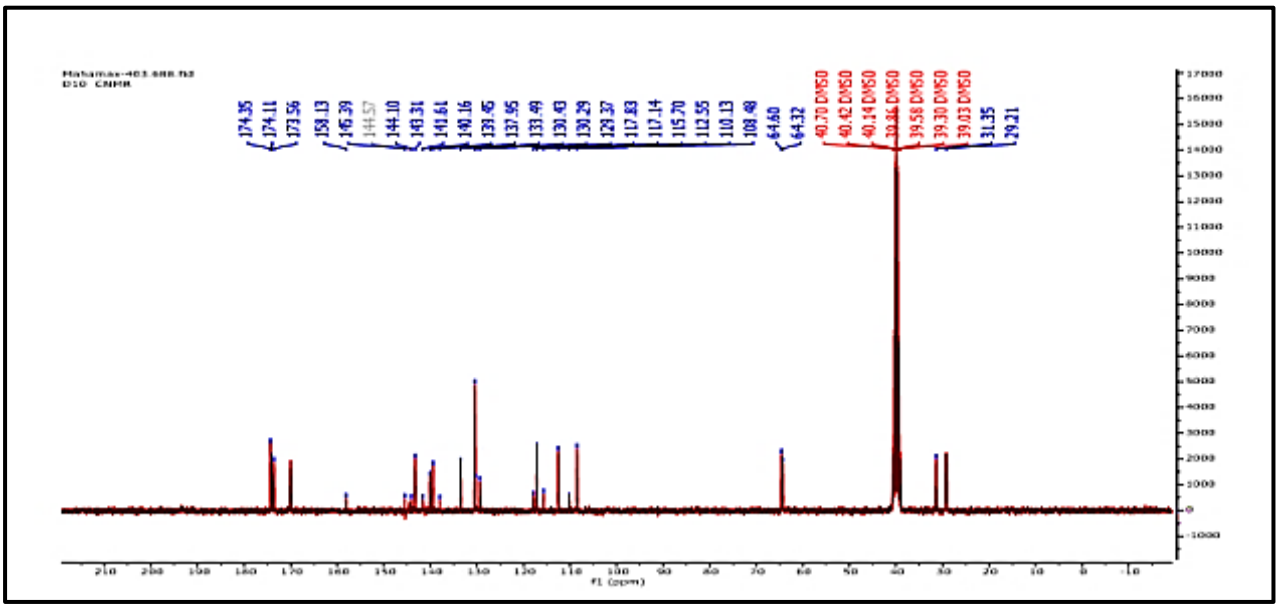

Figure 6: ^{13}C-NMR spectra of the compound (D_1)

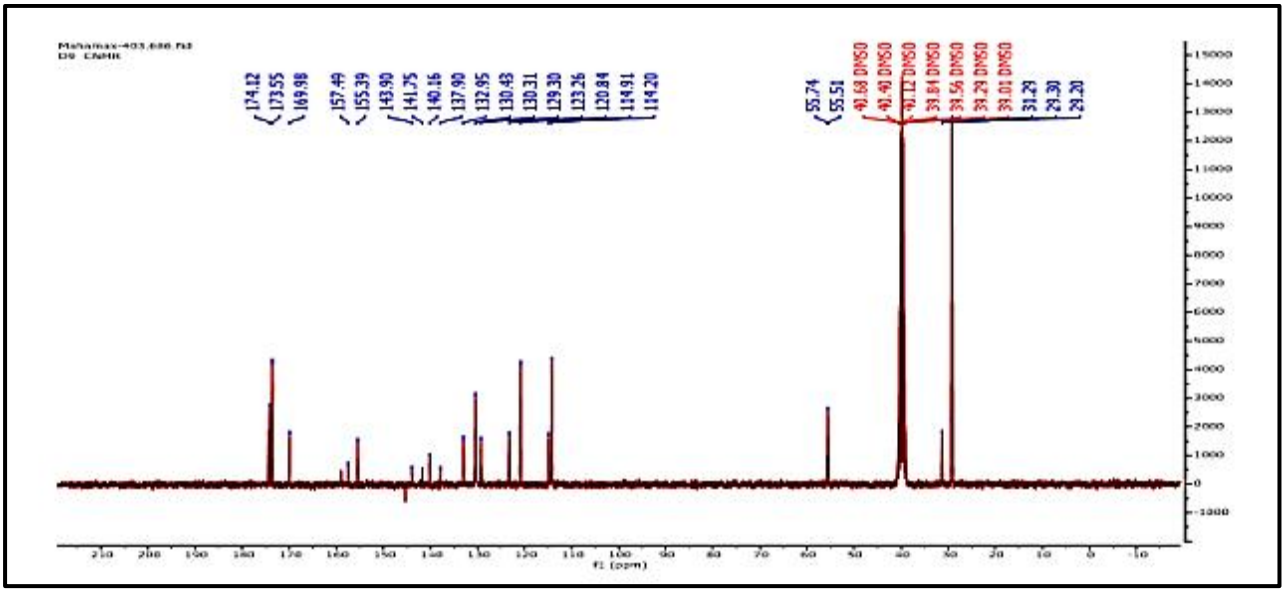

Figure 7: ^{13}C-NMR spectra of the compound (D_3)

Thermogravimetric Analysis (TGA).

Thermogravimetric (TG) analysis was performed on prepared compounds D_1 and D_3 to determine their thermal stabilities and to confirm or deny the presence of water in their structures. In an argon environment, measurements were made at heating rates of 20°C per minute. Figures 8 and 9 show the thermal decomposition curves of compounds D_1 and D_3, respectively. In this analysis, the sample mass (weight %) was measured against the temperature rise (25-600°C) under argon gas (Ar). The weight loss was due to the decomposition of the compounds in three stages. The thermogram of compound D_1 showing three steps of decomposition. In the first step, it indicates a loss of 0.3503 mg (12.25%). This weight loss at temperatures ranging from 25 to 100°C can be attributed to the loss of $4H_2O$ mass. The second step shows the decomposition of compound D_1 at temperatures between 110 and 250 °C with a weight loss of 1.24 mg (43.51%). This weight loss is probably due to the loss of CO_2 and the side chain at position C-3 ($C_9H_7BrNO_2$), thus giving a total missing formula of $C_{10}H_7BrNO_4$. This large weight loss is probably the

beginning of the molecular decomposition of the compound. In the third stage of decomposition, a weight loss of 1.195 mg (41.81%) occurs at temperatures between 250 and 600 °C, possibly involving the loss of the side chain at position C-7(C_6H_5SO) and the remaining beta-lactam-thiazine with the methoxy group (OCH_3), Note Figure 8 and Scheme 2. The remaining weight is 2.5% versus 97%, which may be due to ash resulting from inorganic residues. We conclude that compound D_1 begins to lose weight at low temperatures (100°C), which is probably due to the loss of volatile materials. The decomposition stage of the compound begins at 150°C, which is the temperature at which the compound is thermally stable.

As for the thermal decomposition of compound D_3, the decomposition process takes place in three stages at temperatures of 25-600 ℃. In the first stage, when heated to 25-200℃, it leads to a weight loss of 3.8 mg (46.05%). In this stage, a large decomposition occurs in the compound, perhaps as a result of the loss of the less stable and more reactive groups in the compound. The missing part of the compound may be the side chain at position C-3 ($C_{11}H_{10}ClNO_4$). In the second stage (32.60 %), which begins when heated to 200-310°C, the side chain ($C_{11}H_{10}NOS$)C-7 is likely to be lost. The final stage at 310-600 ℃, in which a weight loss of 1.453 mg (17.59%) occurs, decomposes the remaining organic core structure. Note Figure 9 and Scheme 3. The remaining sample yields 3.75% compared to 96.25%. This small remaining percentage indicates that the compound is mostly organic.

Comparing the two compounds, the thermal analysis results showed a clear difference between them. Compound D_3 exhibited the highest weight loss in the first stage at 46.05%, while the primary decomposition of compound D_1 was concentrated in the second and third stages at 43.51% and 41.61%, respectively. This behavior indicates that D_1 possesses better initial thermal stability, while D_3 begins to decompose at lower temperatures. Regarding byproducts, compound D_3 yielded a carbon residue yield of 3.75%, higher than the 2.63% recorded for compound D_1. Therefore, it can be concluded that the distribution of mass loss in D1 is more pronounced in the later stages compared to compound D_3. Note Figure 11.

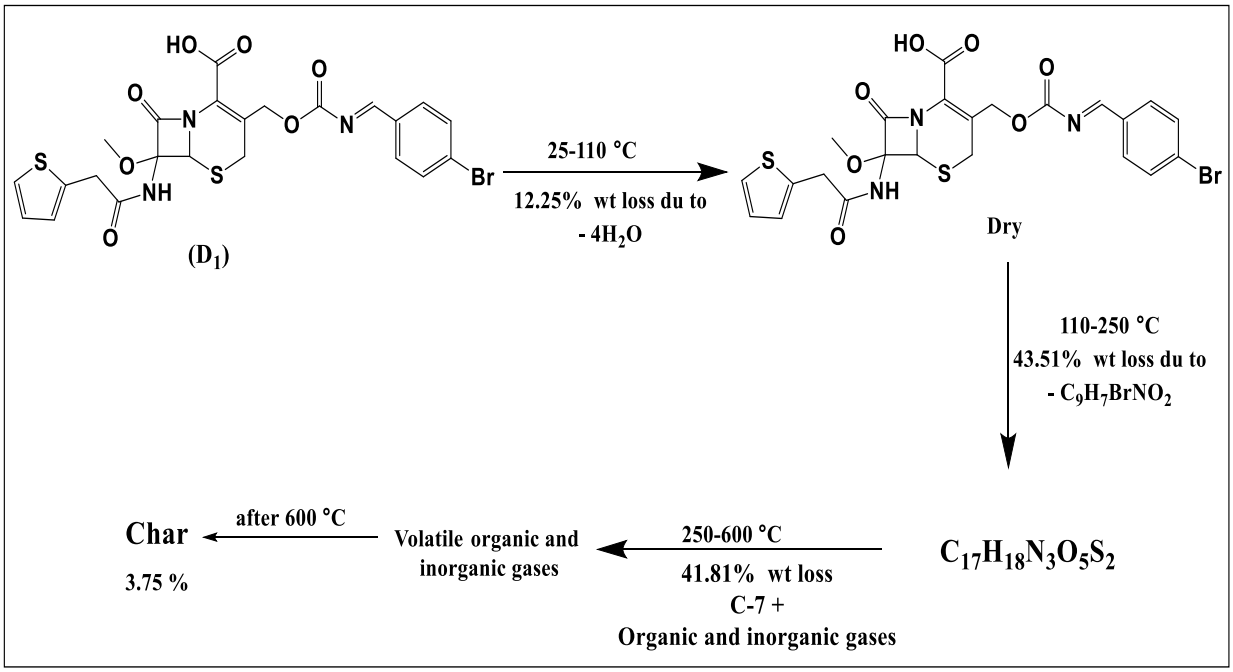

Scheme 2: Decomposition structure of compound D_1 in the presence of an argon atmosphere.

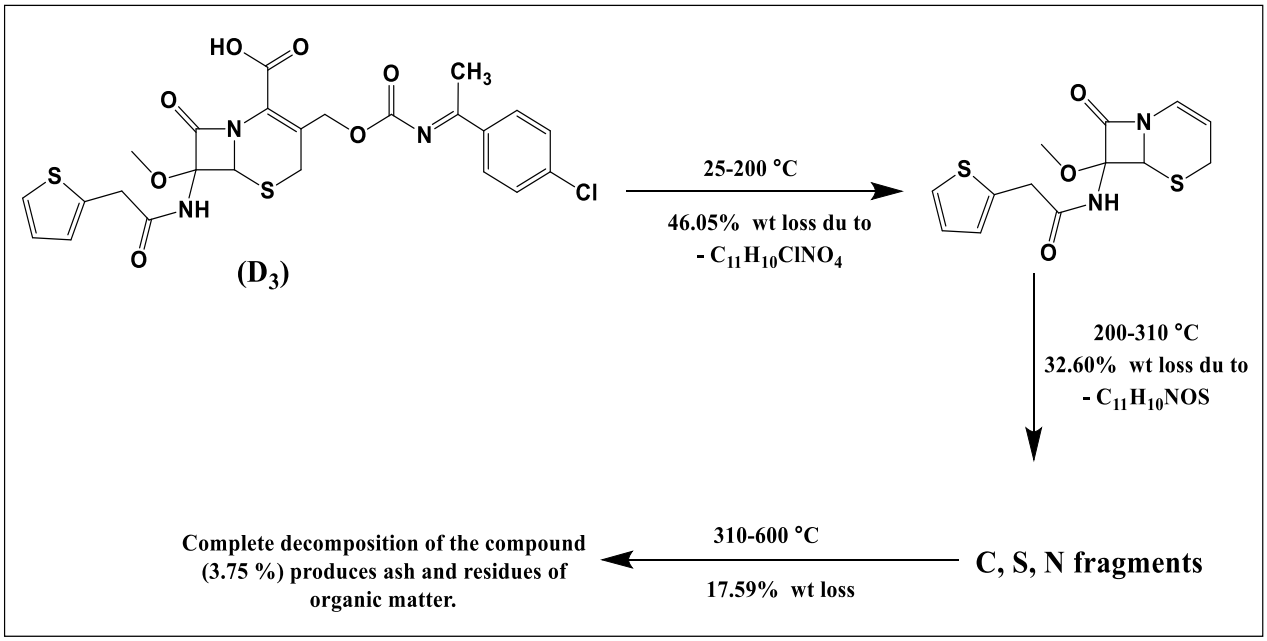

Scheme 3: Decomposition structure of compound D_3 in the presence of an argon atmosphere.

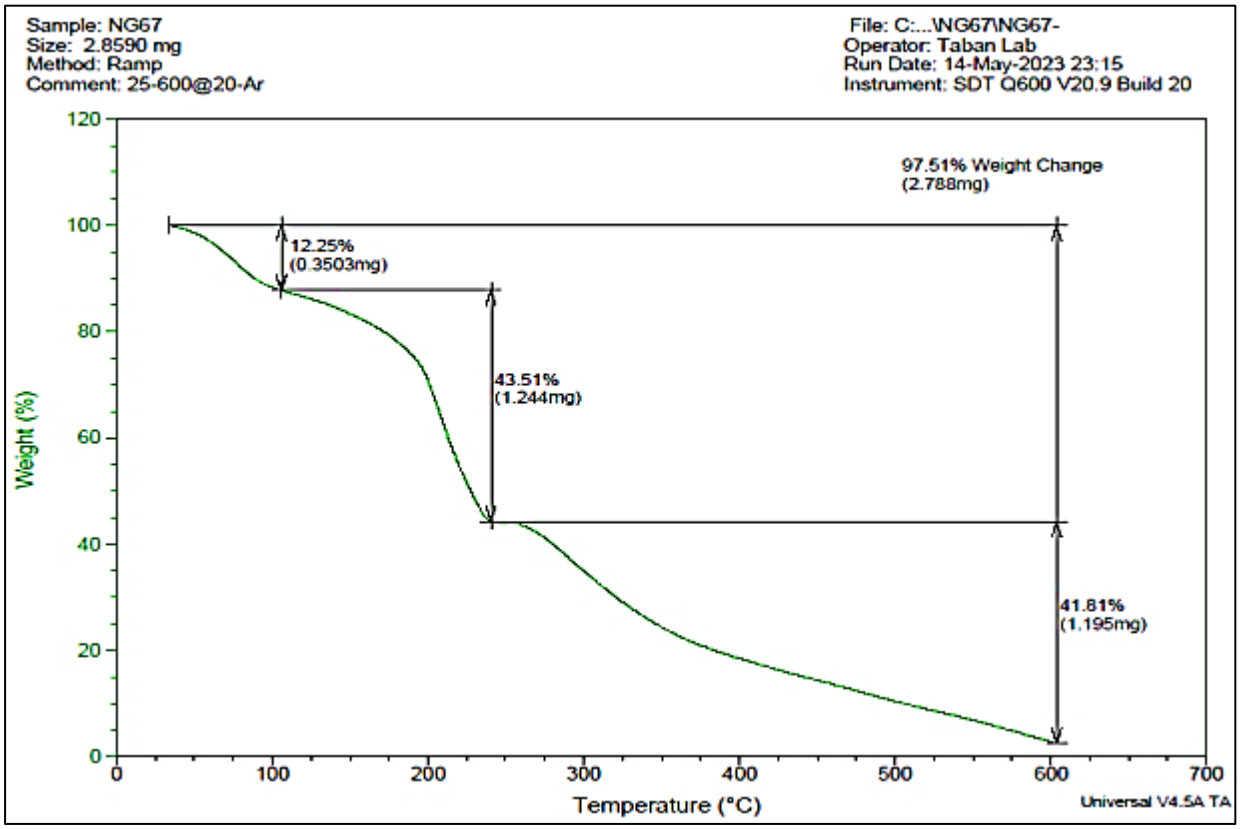

Figure 9: TGA spectrum for compound D_1 in the presence of argon. gas.

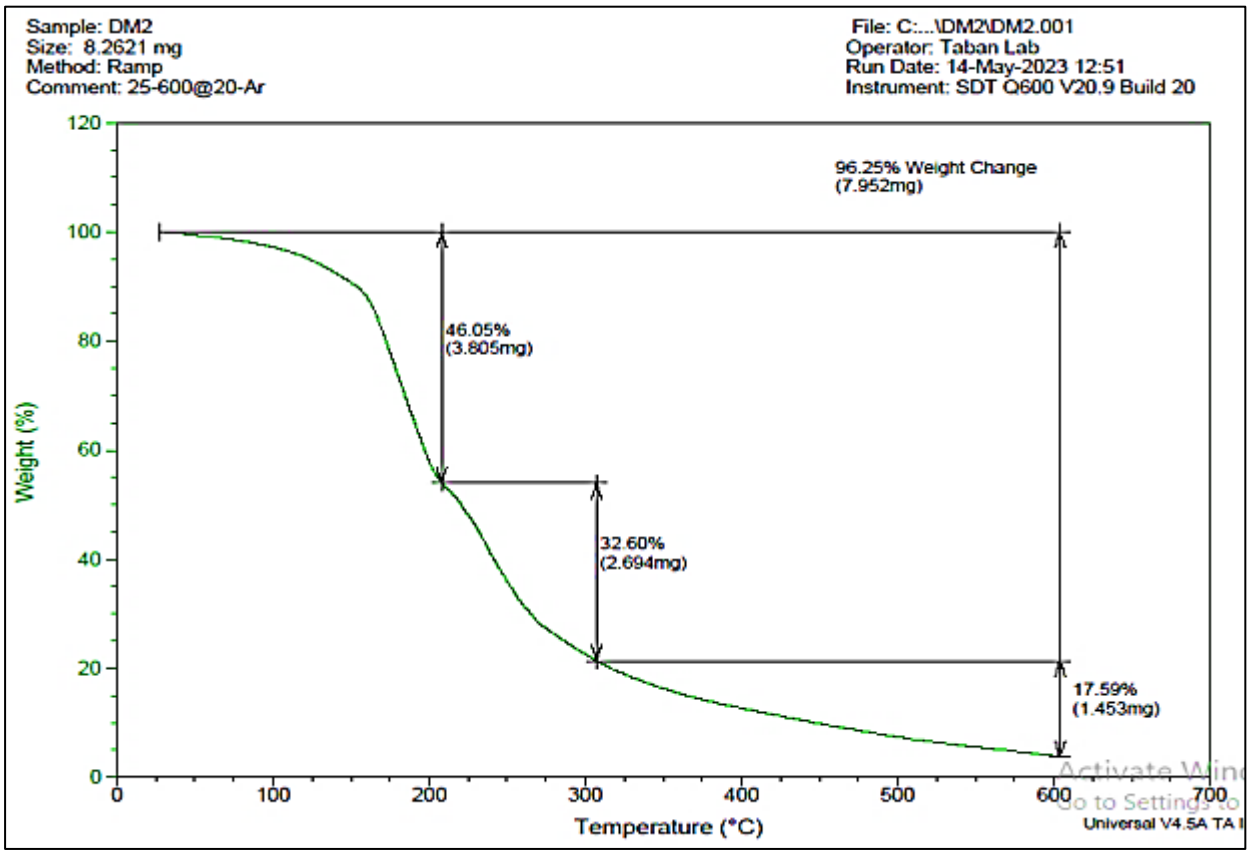

Figure 10: TGA spectrum for compound D_3 in the presence of argon.

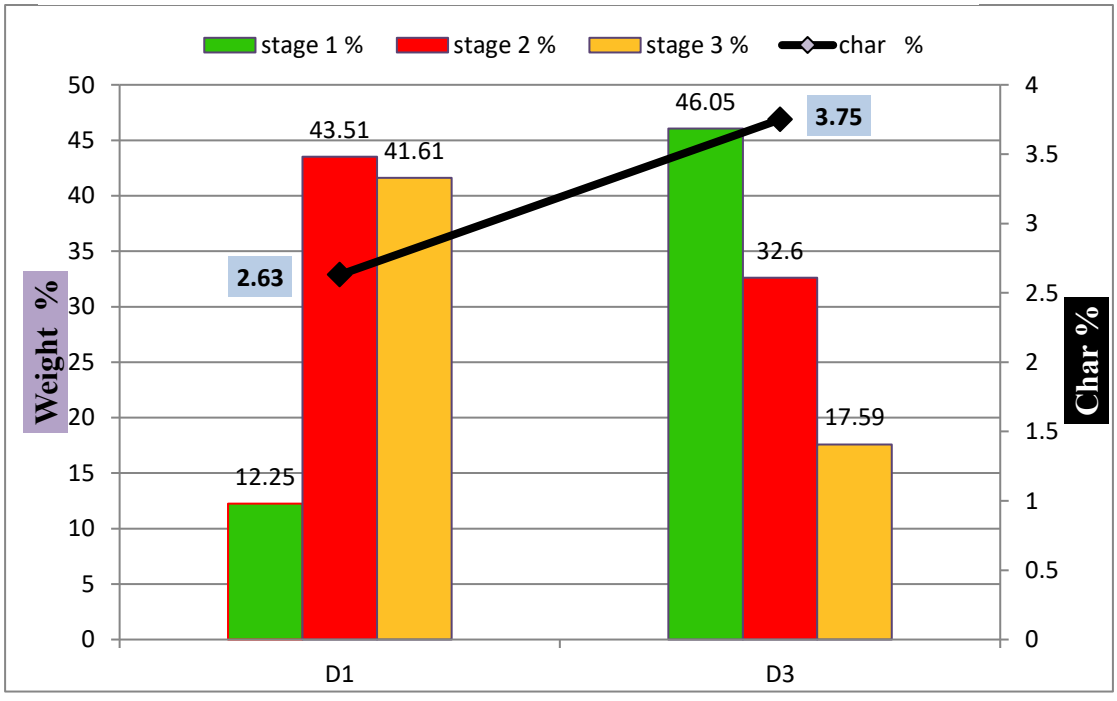

Figure 11: Comparing Compounds D_1, and D_3 in Terms of Weight Loss Stages and Char Yield.

Antibacterial activity assessment.

Each of the resulting compounds, D_1, D_2, D_3, and D_4, was dissolved in DMSO and tested for antibacterial activity against gram-positive bacteria and gram-negative bacteria using the agar diffusion technique. Following that, the plates were incubated for 24 hours at 37°C before analysis. Standard antibiotics like ceftriaxone were used to assess the possible effects of these substances. Everybody compounds

at different concentrations (0.01, 0.001, and 0.0001 mg/mL), using DMSO as a control and a solvent. The inhibition zone diameter in mL(IZD) was computed to quantify the antibacterial activity. Each of the compounds was tested in relation to the control to determine their minimum inhibitory concentration (MIC, g/mL), which is the lowest quantity required to prevent bacteria from multiplying[27, 28], Compound D_3 showed a 40 mm inhibition zone at 0.01 mg/ml against *Klebsiella* bacteria and maintained its high efficacy even at 0.001 mg/ml, with an inhibition zone of 36 mm. This indicates that compound D_3 is highly effective against this type of bacteria compared to the antibiotic gentamicin. While compounds D_2 and D_3 showed favorable activity against *Staphylococcus aureus* and *Enterococcus faecalis* bacteria, respectively, with an inhibition zone diameter of 20 mm, a decrease in the effectiveness of these compounds was observed with decreasing concentrations, indicating that these types of bacteria require high concentrations of the compounds to be effectively inhibited. Compounds D_1, D_3, and D_4 were the least effective against *Enterococcus faecalis*, *Pseudomonas*, and *Staphylococcus aureus* bacteria if the diameter of the inhibition zone reached 14 mm and 10 mm, respectively. The results are displayed in Figures 12, 13, and 14.

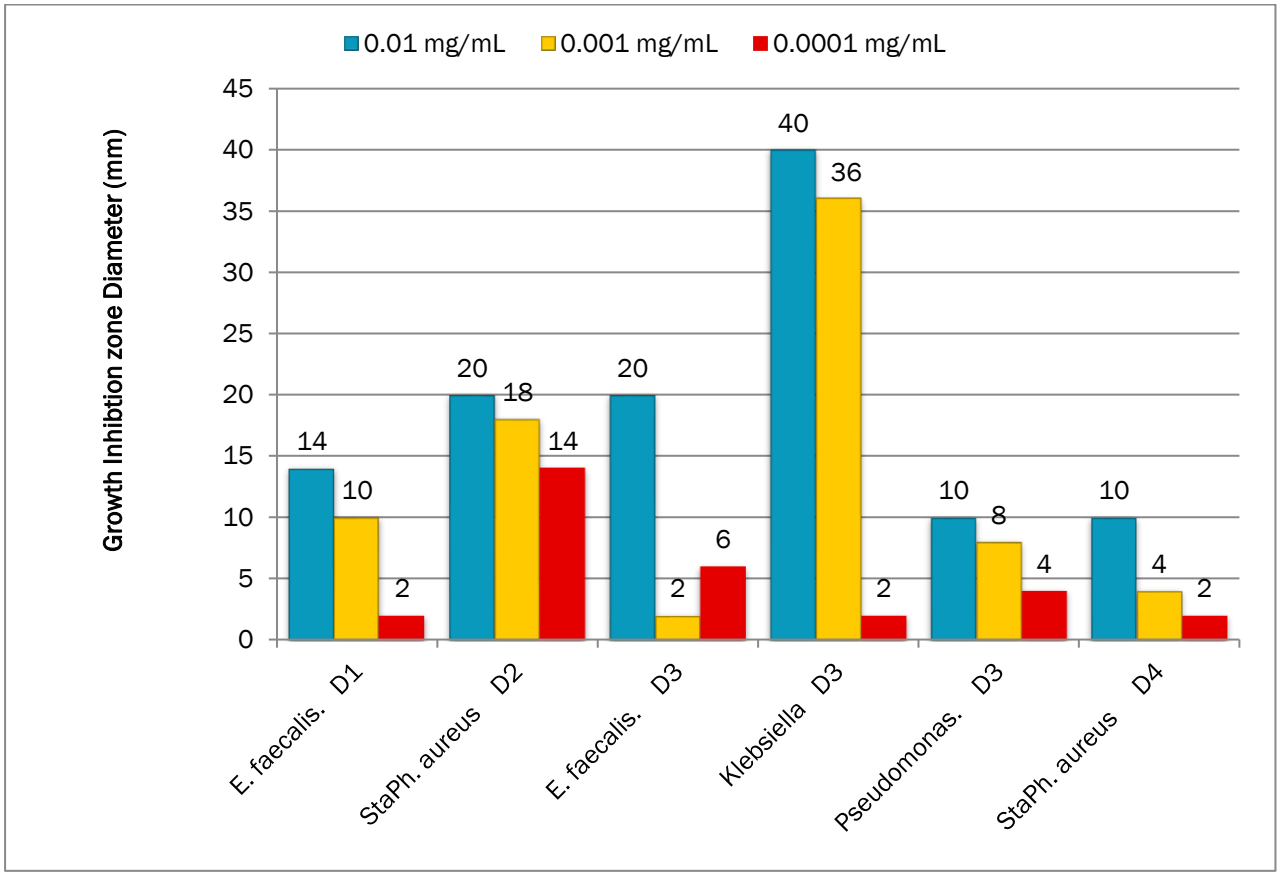

Figure 12: Effect of different concentrations on the growth of bacterial strains.

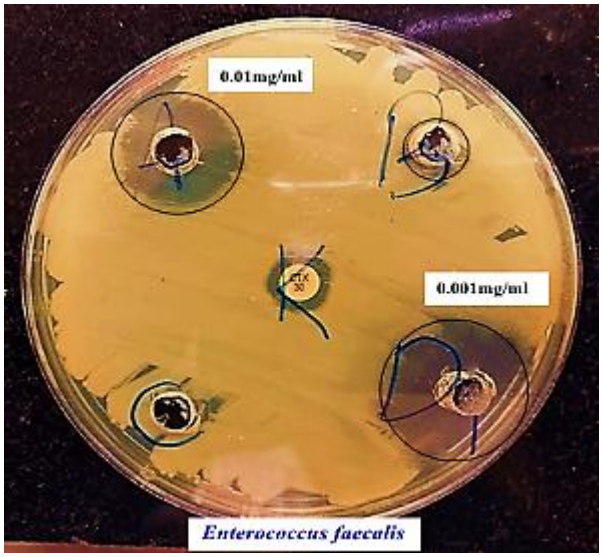

Figure 13(a): Efficacy of compound D_1 against *Enterococcus faecalis*

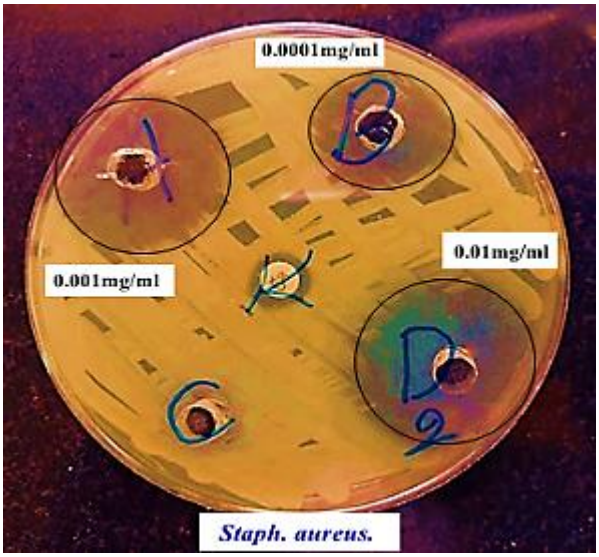

Figure 13(b): Efficacy of compound D_2 against *Staphylococcus aureus.*

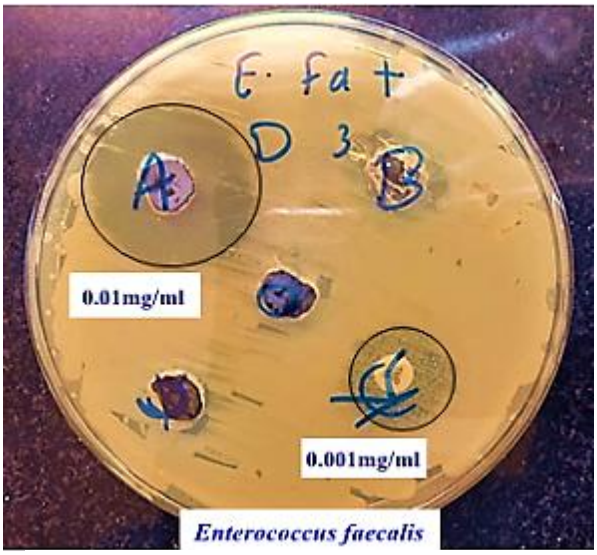

Figure 14(b): Efficacy of compound D_3 against *Enterococcus faecalis.*

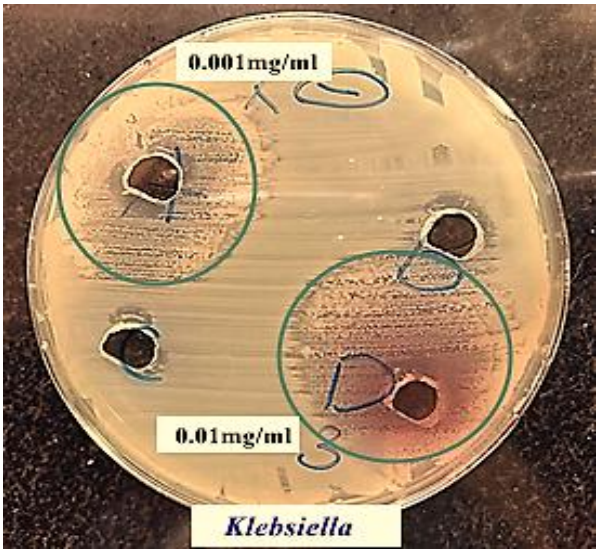

Figure 14(a): Efficacy of compound D_3 against *Klebsiella*.

Molecular Docking.

The new compounds (D_2 and D_3) were synthesized and described for use in molecular docking. To generate the three-dimensional structures of the compounds, ChemDraw Ultra 12.0 (Figure 15)[29] was used. Using the Austin Model 1 method, the structures of the compounds were optimized by Hyperchem 8.08[30]. To obtain the most stable configuration, the B3LYP/6-31G basis set was used based on density functional theory[31]. The crystal structure of protein 8C7Y was selected from the Protein Data Bank. A water molecule was added to the protein's active site to form hydrogen bonds between the ligand and the target. Using X-ray diffraction, the missing bonds were corrected to prepare the protein structure, followed by the addition of hydrogen atoms. The Molecular Operating Environment (MORE) software was used to merge the optimized compound structures into a single database, and all docking and scoring calculations were performed[1]. The protein crystal structure was obtained from the Protein Data Bank at a resolution of 1.65 Å.

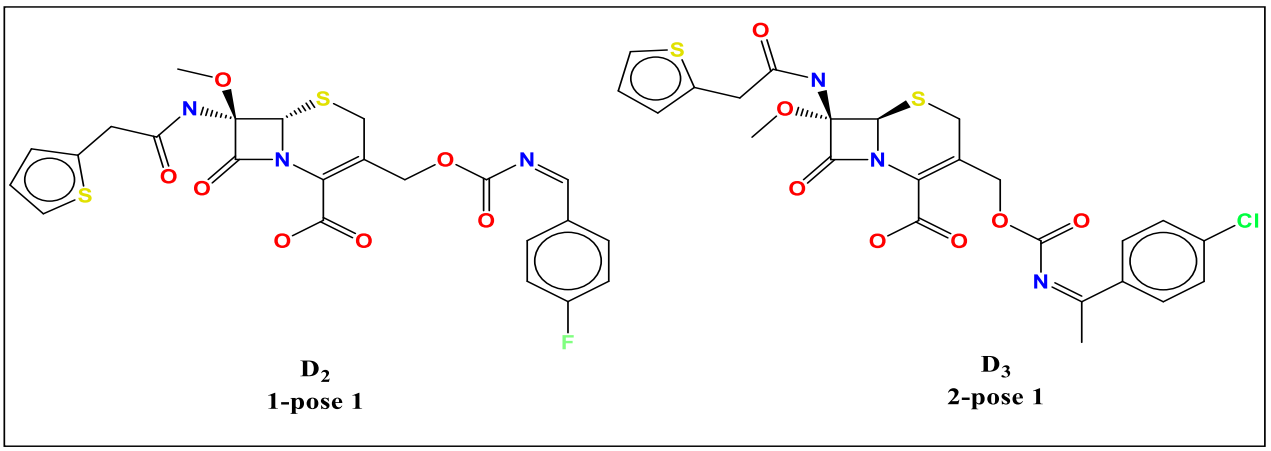

Figure 15: 2D structures of selected compounds (ligands).

Results.

Molecular docking is used as a fundamental tool in the drug discovery pipeline. In the present study, MOE software was applied to perform all molecular docking calculations and predict the binding modes of the prepared compounds (D_2 and D_3) with the protein (8C7Y). The predicted binding affinities and features of the investigated compounds toward 8C7Y are listed in the next tables. These tables show the best binding poses of compounds against target proteins. The 2D and 3D representations of interactions of the inspected compounds with the key amino acid residues of the 8C7Y proteins are illustrated in the next figures and tables. Compounds (D_2 and D_3) showed good binding affinity values with proteins (8C7Y). It shows the presence of different interactions through the association of compounds with the protein in 2D and 3D forms. Among these interactions are hydrophobic interactions and hydrogen bonds. Interactions were further examined for bond lengths and hydrogen bonds in the active site. The results showed that compounds (D_2 and D_3) interact with different amino acid residues in three different interactions: H-donor, H-acceptor, and H-pi, as well as two H-acceptor and pi-H interactions with the water and different amino acids. See Figure 16-18 and Tables 3-4.

Table 3: rmsd value and binding affinity of compounds containing 8C7Y.

Pose of Compounds	mseq	Binding Affinity Kcal/mol	Rmsd (Å)	Energy conf.	Energy Place.	Energy score1.	Energy Refine.	Energy score2
1- pose1	1	-9.91703	2.02946	44.91108	-17.4953	-10.3758	-53.587	-9.91703
1- pose2	1	-9.73725	4.05983	54.24571	-14.1242	-8.54153	-47.2592	-9.73725
1- pose 3	1	-9.48318	1.611473	46.81051	-14.1968	-10.3108	-49.4706	-9.48318
1- pose4	1	-9.334	1.694666	50.00678	-17.5819	-11.453	-43.0345	-9.334
1- pose5	1	-9.11034	1.93809	40.77024	-14.1835	-10.2601	-49.2388	-9.11034
2- pose1	2	-9.78675	2.776514	33.81412	-17.6737	-12.1898	-46.6228	-9.78675
2- pose2	2	-9.62109	2.092845	50.62668	-15.7711	-11.5144	-52.4773	-9.62109
2- pose3	2	-9.50213	2.049769	32.68086	-21.2859	-11.6363	-41.0556	-9.50213
2- pose4	2	-9.25896	1.637712	72.28388	-18.0064	-12.532	-38.5546	-9.25896
2- pose5	2	-9.24248	1.72728	71.88135	-16.5379	-11.7473	-37.6427	-9.24248
standard	std	-8.62212	1.924656	72.87959	-39.381	-12.2215	-56.3795	-8.62212

Table 4: The best pose for protein 8C7Y

Pose of Compounds	Binding Affinity Kcal/mol	RMSD (Å)	The compound's Atom	Receptor Atom	Receptor residues Involved	Interaction bond type	Distance (Å)	E (kcal/mol)
1- pose1	-9.917	2.029	S 17	OD2	ASP 594	H. Bond -acceptor	4.39	-0.8
			S 17	OD2	ASP 594	H. Bond -donor	4.23	-1
			S 7	N	ASP 594	H. Bond -acceptor	3.14	-3.2
			S 7	N	ASP 594	H. Bond -acceptor	3.14	-3.2
			O 12	OG	SER 467	H. Bond -acceptor	2.76	-0.6
			O 12	OG	SER 467	H. Bond -acceptor	2.96	-0.5
			O 14	NZ	LYS 483	H. Bond -acceptor	2.36	7.9
			O 14	NZ	LYS 483	H. Bond -acceptor	2.71	-3
			O 28	NZ	LYS 483	H. Bond -acceptor	3.52	-1.1
			F 36	N	CYS 532	H. Bond -acceptor	2.95	-0.4
			F 36	N	CYS 532	H. Bond -acceptor	2.95	-0.4
			5-ring	5-ring	HIS 574	B- pi-pi	3.88	0
2- pose2	-9.621	2.092	S 7	CA	PHE 595	H. Bond -acceptor	4.07	-0.4
			S 7	CA	PHE 595	H. Bond -acceptor	4.07	-0.4
			O 14	CE	LYS 483	H. Bond -acceptor	3.19	-1.3
			O 14	CE	LYS 483	H. Bond -acceptor	3.26	-1.1
			O 16	N	CYS 532	H. Bond -acceptor	3.27	-0.4
			O 16	SG	CYS 532	H. Bond -acceptor	3.01	-0.9
			O 16	SG	CYS 532	H. Bond -acceptor	3.22	-1.5
			5-ring	6-ring	TRP 531	B- pi-pi	3.81	0
			5-ring	6-ring	TRP 531	B- pi-pi	3.95	0
standard	-8.622	1.924	N1 1	OE2	GLU 501	H. Bond -donor	2.84	-5.5
			N2 6	O	GLN 530	H. Bond -donor	2.87	-5.0
			O1 10	O	HOH 913	H. Bond –acceptor	2.68	-2.4
			N3 16	N	CYS 532	H. Bond -acceptor	2.91	-5.3

Figure 16: 2D and 3D interaction Model of the Compound D_2 with Protein 8C7Y.

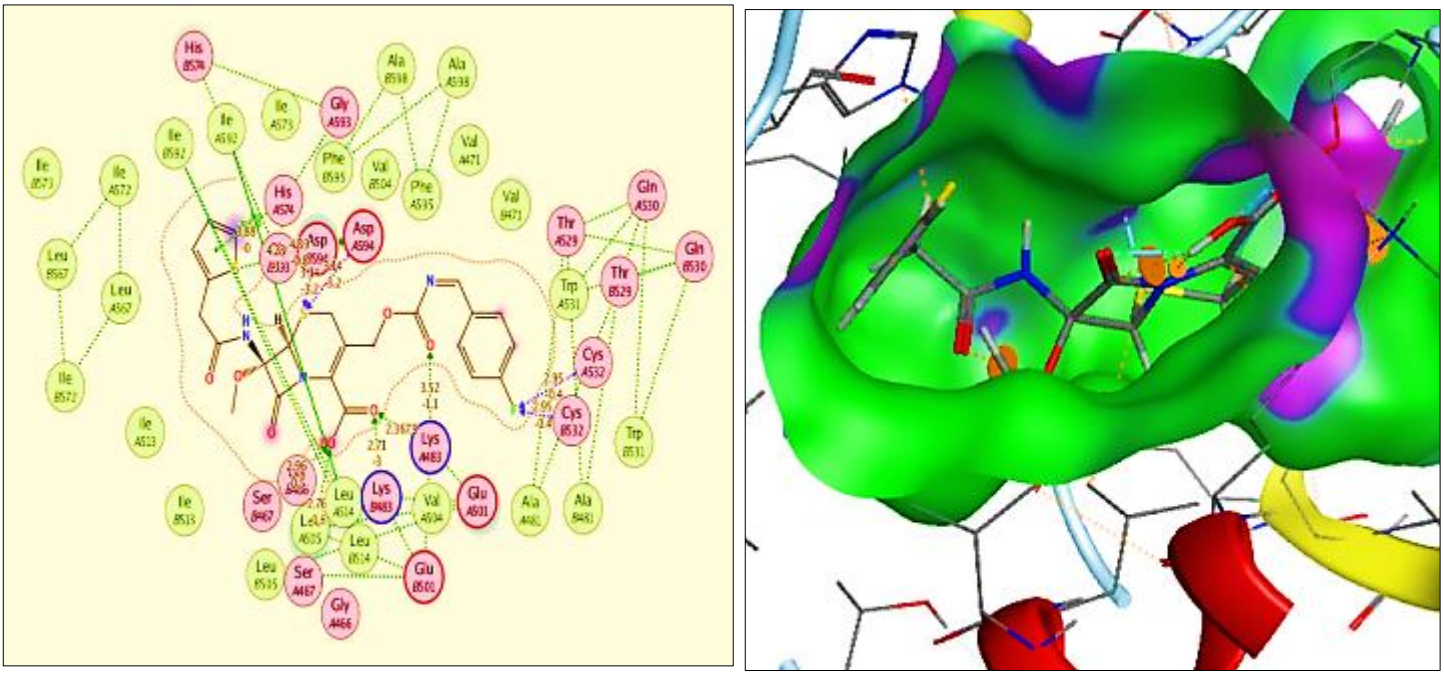

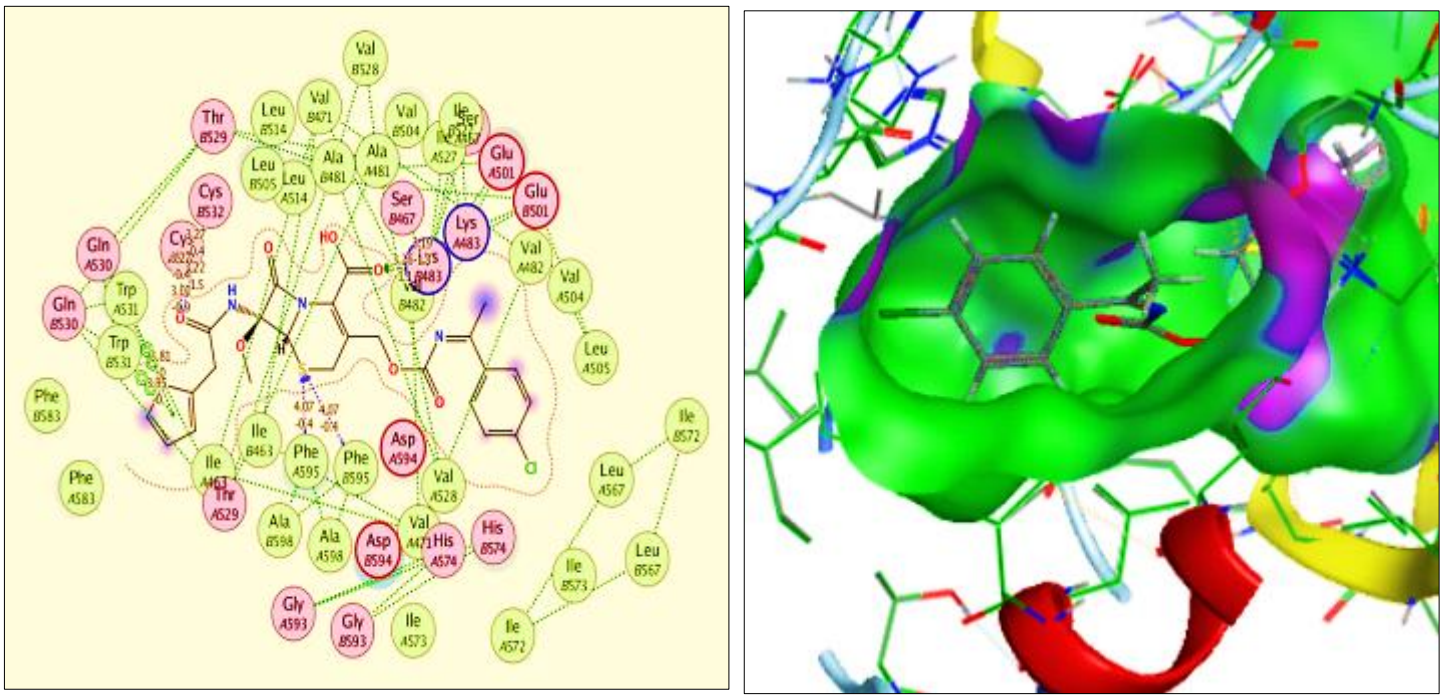

Figure 17: 2D and 3D interaction Model of the Compound D_3 with Protein 8C7Y.

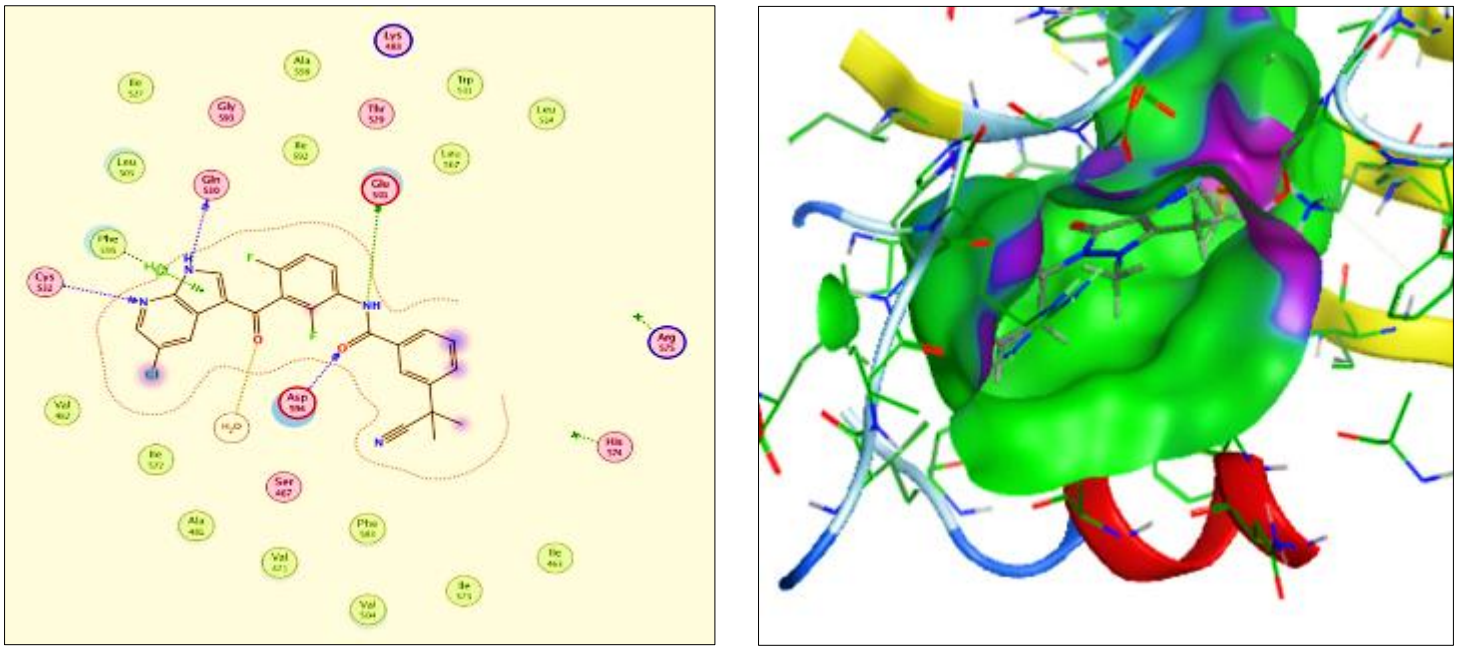

Figure 18: 2D and 3D interaction Model of the Standard with Protein 8C7Y.

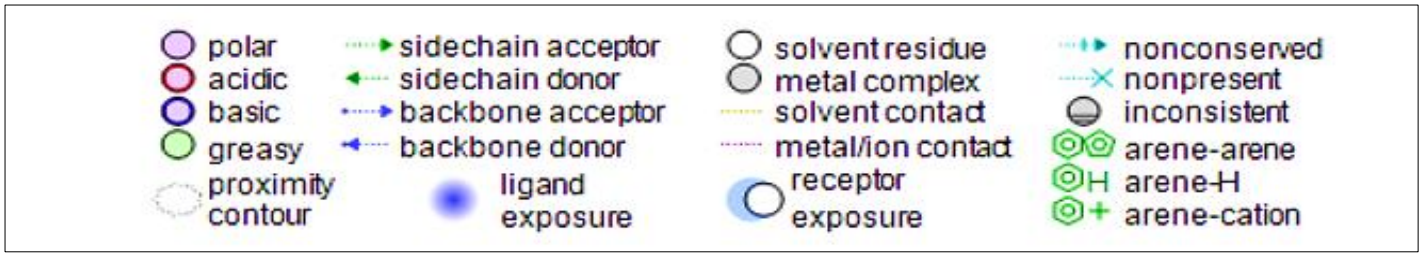

Interpretation of molecular docking results.

The pose collection is split into series. The top tier comprises the best of series-2 and series-1. 2-pose2 (−9.62 kcal/mol, RMSD 2.09 Å) and 1-pose1 (−9.92 kcal/mol, RMSD 2.03 Å) both outperform the standard by ~1–1.3 kcal/mol. In 2-pose2, the per-residue map indicates repeated H-acceptor contacts with PHE595, LYS483, and CYS532 plus π-π stacking with TRP531, giving it strong placement (−15.77 kcal/mol) and very favorable refined energy (−52.48 kcal/mol). 1-pose1 forms a large hydrogen-bond cluster to ASP594 and SER467 and several π- H interactions with THR347/LEU525; there is a single positive term with LYS483 that looks like a steric/electrostatic penalty, but it is outweighed by multiple donors and acceptors within 2.7–3.2 Å, which is why its net binding remains strong. All top poses have RMSDs ~2.0–2.1 Å, comparable to the standard (1.92 Å), so these improvements in ΔG are not artifacts of distorted geometries. Within each series the trend is consistent: moving down each block from pose1 to pose5 weakens the affinity and often raises RMSD, suggesting the search engine is sampling the same pocket with gradually worse orientations. The standard itself binds reasonably (−8.62 kcal/mol), but it relies more on refinement energy and pays a larger conformational/placement cost; that profile is typical for a bulky scaffold that fits but does not pack optimally. In conclusion, Series-2 provides credible candidates led by 2-pose-2, and Series-1's best pose is competitive and chemically instructive because of its strong H-bond network even in the presence of a mild electrostatic clash .The bars show binding affinity (more negative is better; axis inverted) for all poses in blue (series-1), amber (series-2), and grey (standard). The black line overlays RMSD. Note Figure 19.

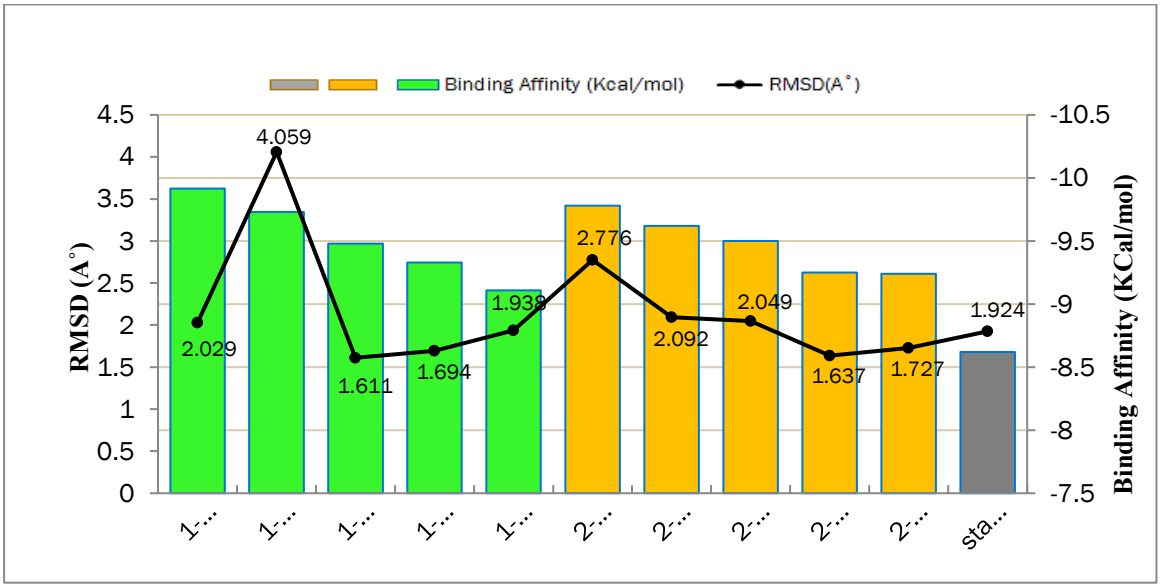

Figure 19: 8C7Y Docking Poses: Binding Affinity and RMSD Comparison.

Conclusion

Derivatives of Schiff bases have high biological activity and are of great academic significance for applications in medicine. Cefoxitin has been effectively used to create new Schiff base derivatives by addition and condensation reactions with substituted benzaldehydes or ketones in an acidic medium. Spectral diagnostic results were consistent with the structural properties of the synthesized compounds. Biological activity results showed that the synthesized compounds were effective against various types of bacteria, including Pseudomonas aeruginosa, Klebsiella, Staphylococcus aureus, and Enterococcus faecalis, at high

concentrations compared to low concentrations. Compound D_2 showed a strong effect against Staphylococcus aureus, while compound D_3 showed a strong effect against Klebsiella bacteria. The thermal decomposition of compounds D_1 and D_3 was carried out in three stages at temperatures of 25-600°C. The first stage is the weight loss of compound D_1 due to the loss of volatile solvents or moisture. In stages two and three, it became mere organic decomposition. Compound D_1 was stable in the gradual decomposition, but compound D_3 showed sharp decomposition at 110–200 °C with a total weight loss of 65% for compound D_3 and of 97% for strain D_1. This indicates that compound D_3 is more thermally stable or may contain stable carbonaceous materials. The MOE program's molecular docking studies showed that chemicals D_2 and D_3 bind to the protein 8C7Y with great efficiency and strong affinity values. Important interactions, including hydrophobic and hydrogen bonding interactions with the essential amino acid residues, are revealed by the interaction patterns. The highest binding affinity shown for the 3-pose-1 conformation (-10.56 Kcal/Mol) is superior to that of the standard inhibitor (-8.62 Kcal/Mol) due to the ideal localization within the active site. The 1-pose 1 and 2-pose-2 conformations also form superior complexes to the standard compound.

REFERENCES

[1] K. Shahbaz, "Cephalosporins: pharmacology and chemistry," *Pharmaceutical and Biological Evaluations*, 2017.

[2] I. Naqvi, A. Saleemi, and S. Naveed, "Cefixime: A drug as Efficient Corrosion Inhibitor for Mild Steel in Acidic Media. Electrochemical and Thermodynamic Studies," *Int. J. Electrochem. Sci.*, vol. 6, no. 1, pp. 146–161, 2011, doi: 10.1016/s1452-3981(23)14982-0.

[3] M. Gurwith, W. Albritton, B. Lank, G. Harding, and A. Ronald, "Comparison of cefoxitin sodium and cefazolin," *J. Antimicrob. Chemother.*, vol. 4, no. suppl_B, pp. 211–213, 1978, doi: 10.1093/jac/4.suppl_b.211.

[4] T. A. Antonenko *et al.*, "Biological activity of novel organotin compounds with a Schiff base containing an antioxidant fragment," *Int. J. Mol. Sci.*, vol. 24, no. 3, p. 2024, 2023.

[5] J. Sóki, S. M. Gonzalez, E. Urbán, E. Nagy, and J. A. Ayala, "Molecular analysis of the effector mechanisms of cefoxitin resistance among Bacteroides strains," *J. Antimicrob. Chemother.*, vol. 66, no. 11, pp. 2492–2500, 2011, doi: 10.1093/jac/dkr339.

[6] J. Yu, L.-b. Jiang, W.-d. Feng, C.-m. Zhao, and F.-l. Zhang, "Preparation of three impurities in cefoxitin," *J. Chem. Res.*, vol. 42, no. 11, pp. 541–546, 2018, doi: 10.3184/174751918x15402956899595.

[7] D. W. Bratzler, P. M. Houck, and S. I. P. G. W. Workgroup, "Antimicrobial prophylaxis for surgery: an advisory statement from the National Surgical Infection Prevention Project," *Am. J. Surg.*, vol. 189, no. 4, pp. 395–404, 2005, doi: 10.1016/j.amjsurg.2005.01.015.

[8] P. Moine, S. W. Mueller, J. A. Schoen, K. B. Rothchild, and D. N. Fish, "Pharmacokinetic and pharmacodynamic evaluation of a weight-based dosing regimen of cefoxitin for perioperative surgical prophylaxis in obese and morbidly obese patients," *Antimicrob. Agents Chemother.*, vol. 60, no. 10, pp. 5885–5893, 2016, doi: 10.1128/aac.00585-16.

[9] I. Mushtaq, M. Ahmad, M. Saleem, and A. Ahmed, "Pharmaceutical significance of Schiff bases: an overview," *Future J. Pharm. Sci.*, vol. 10, no. 1, p. 16, 2024, doi: 10.1186/s43094-024-00594-5.

[10] S. K. Raju, A. Settu, A. Thiyagarajan, D. Rama, P. Sekar, and S. Kumar, "Biological applications of Schiff bases: An overview," *GSC Biol. Pharm. Sci.*, vol. 21, no. 3, pp. 203–215, 2022, doi: 10.30574/gscbps.2022.21.3.0484.

[11] V. Manvatkar, R. Patle, P. Meshram, and R. Dongre, "Azomethine-functionalized organic–inorganic framework: an overview," *Chem. Pap.*, vol. 77, no. 10, pp. 5641–5662, 2023, doi: 10.1007/s11696-023-02889-y.

[12] M. Li *et al.*, "Nitrogen-doped porous carbon nanosheets based on a Schiff base reaction for high-performance lithium-ion batteries anode," *Energies*, vol. 16, no. 4, p. 1733, 2023.

[13] S. S. Mukhtar, A. S. Hassan, N. M. Morsy, T. S. Hafez, H. M. Hassaneen, and F. M. Saleh, "Overview on synthesis, reactions, applications, and biological activities of Schiff bases," *Egypt. J. Chem.*, vol. 64, no. 11, pp. 6541–6554, 2021, doi: 10.21608/ejchem.2021.79736.3920.

[14] J. Ceramella, D. Iacopetta, A. Catalano, F. Cirillo, R. Lappano, and M. S. Sinicropi, "A review on the antimicrobial activity of Schiff bases: Data collection and recent studies," *Antibiotics*, vol. 11, no. 2, p. 191, 2022, doi: 10.3390/antibiotics11020191.

[15] M. S. Tople, N. B. Patel, P. P. Patel, A. C. Purohit, I. Ahmad, and H. Patel, "An in silico-in vitro antimalarial and antimicrobial investigation of newer 7-chloroquinoline based Schiff-bases," *J. Mol. Struct.*, vol. 1271, p. 134016, 2023, doi: 10.1016/j.molstruc.2022.134016.

[16] V. J. Kumar *et al.*, "Identification, isolation and characterization of a new impurity in cefoxitin drug substance resulting from stress stability studies," *Anal. Methods*, vol. 3, no. 1, pp. 181–185, 2011.

[17] R. Sahu and K. Shah, "Schiff bases: a captivating scaffold with potential anticonvulsant activity," *Mini Rev. Med. Chem.*, vol. 24, no. 18, pp. 1632–1650, 2024, doi: 10.2174/0113895575302197240408121537.

[18] A. M. Naglah *et al.*, "Exploring the potential biological activities of pyrazole-based Schiff bases as anti-diabetic, anti-Alzheimer's, anti-inflammatory, and cytotoxic agents: in vitro studies with computational predictions," *Pharmaceuticals*, vol. 17, no. 5, p. 655, 2024, doi: 10.3390/ph17050655.

[19] M. A. Mseer, K. Jawad, and Y. Al-Khafaji, "Synthesis and Characterization of Heterocyclic Compounds Derived from Schiff base Glycerol Triester," *NeuroQuantology*, vol. 19, no. 9, pp. 88–96, 2021, doi: 10.14704/nq.2021.19.9.nq21141.

[20] S. Beebany, S. S. Jasim, M. M. Al-Tufah, and S. Arslan, "Preparation and identification of new 1,4-bis(5,3-substituted-2,3-dihydro-1H-pyrazole-1-yl) Buta-1,4-Dione derivatives with their antibacterial effect evaluation," *Chem. Methodol.*, vol. 7, pp. 123–136, 2023.

[21] M. M. Al-Tufah, K. A. Al-Badrany, and S. S. Jasim, "Synthesis and antibacterial evaluation of some New 1,5-Benzooxazepines derivatives," *Syst. Rev. Pharm.*, vol. 12, no. 3, pp. 270–285, 2021.

[22] W. Y. Cun, P. A. Keller, and S. G. Pyne, "Synthesis of 7α-Methoxy-7-(4-phenyl-1 H-1,2,3-triazol-1-yl) acetamino-3′-arylthio-cephalosporic Acid Derivatives from 7-Aminocephalosporic Acid," *Molecules*, vol. 28, no. 21, p. 7338, 2023, doi: 10.3390/molecules28217338.

[23] R. El-Zawawy, M. Masoud, A. Ali, and M. Mosa, "Synthesis, structural, DFT, solid state and antimicrobial studies of some new biologically active cefoxitin complexes," *Inorg. Chem. Commun.*, vol. 121, p. 108218, 2020, doi: 10.1016/j.inoche.2020.108218.

[24] J. R. Anacona and C. C. Gil, "Synthesis and antibacterial activity of cefoxitin metal complexes," *Transition Met. Chem.*, vol. 30, no. 5, pp. 605–609, 2005, doi: 10.1007/s11243-005-3847-3.

[25] M. A. El-Atawy, E. A. Hamed, M. Alhadi, and A. Z. Omar, "Synthesis and antimicrobial activity of some new substituted quinoxalines," *Molecules*, vol. 24, no. 22, p. 4198, 2019, doi: 10.3390/molecules24224198.

[26] K. A. Attia, O. Abdel-Aziz, N. Magdy, and G. F. Mohamed, "Determination of cefoxitin sodium in the presence of its alkali-induced degradation product through different ratio spectra manipulating methods," *Anal. Chem. Lett.*, vol. 7, no. 2, pp. 201–214, 2017, doi: 10.1080/22297928.2017.1310631.

[27] M. M. Al-Tufah, S. Beebaeny, S. S. Jasim, and B. L. Mohammed, "Synthesis, characterization of ethyl dioxoisoindolinyl cyclohexenone carboxylate derivatives from some chalcones and its biological activity assessment," *Chem. Methodol.*, vol. 7, pp. 408–418, 2023.

[28] M. F. Gonzalez, F. Magdama, L. Galarza, D. Sosa, and C. Romero, "Evaluation of the sensitivity and synergistic effect of Trichoderma reesei and mancozeb to inhibit under in vitro conditions the growth of Fusarium oxysporum," *Communic. Integr. Biol.*, vol. 13, no. 1, pp. 160–169, 2020, doi: 10.1080/19420889.2020.1829267.

[29] H. K. Al-Ruba, "Synthesis, Antibacterial, and Anticancer Evaluation of Novel Imine Derivatives of 6-Aminopenicillins," *Iraqi J. Biosci. Biomed.*, vol. 2, no. 1, pp. 150–170, 2025.

[30] K. Arora, "In-silico Studies of Simulated IR Spectra of Some Selected Pyrazolone Compounds," *Int. J. Comput. Theor. Chem.*, vol. 11, no. 1, pp. 1–18, 2023, doi: 10.11648/j.ijctc.20231101.11.

[31] H. Kruse, L. Goerigk, and S. Grimme, "Why the standard B3LYP/6-31G* model chemistry should not be used in DFT calculations of molecular thermochemistry: understanding and correcting the problem," *J. Org. Chem.*, vol. 77, no. 23, pp. 10824–10834, 2012, doi: 10.1021/jo302156p.